Applied Catalysis B: Environmental 170-171 (2015) 25–33

Contents lists available at ScienceDirect

Applied Catalysis B: Environmental

journal homepage: www.elsevier.com/locate/apcatb

Insight into the photocatalytic activity of ZnCr–CO_3 LDH and derived mixed oxides

Šárka Paušová[a,b,c,d], Josef Krýsa[c], Jaromír Jirkovský[d], Claude Forano[a,b], Gilles Mailhot[a,b], Vanessa Prevot[a,b,*]

[a] Clermont Université, Université Blaise Pascal, Institut de Chimie de Clermont-Ferrand, BP 10448, F-63000 Clermont-Ferrand, France
[b] CNRS, UMR6296, ICCF, BP 80026, F-63171 Aubière, France
[c] Institute of Chemical Technology Prague, Technicka 5, 166 28 Prague, Czech Republic
[d] J. Heyrovský Institute of Physical Chemistry, Dolejškova 3, 182 23 Prague, Czech Republic

ARTICLE INFO

Article history:
Received 3 November 2014
Received in revised form 14 January 2015
Accepted 21 January 2015
Available online 24 January 2015

Keywords:
Photocatalysis
Layered double hydroxides
Mixed oxides
Orange II
Photodegradation

ABSTRACT

ZnCr–CO_3 layered double hydroxide (LDH) has been prepared by a two-step process combining direct coprecipitation and anionic exchange. To investigate the influence of thermal treatment on ZnCr–CO_3 LDH photocatalytic activity, the thermal decomposition of the matrix was studied by *in-situ* thermal X-ray diffraction and thermal analysis (TGA/DTA). The structure and the textural properties of the materials obtained upon different thermal treatment have been characterized by several techniques such as X-ray diffraction, FTIR, UV–vis diffuse reflectance spectroscopy, N_2 adsorption, scanning and transmission electronic microscopy. Prior to study Orange II (OII) photodegradation, adsorption behavior of uncalcined and calcined ZnCr–CO_3 LDH toward OII was studied evidencing that LDH thermal decomposition leads to a net decrease of the adsorption behavior. All the samples induce the photodegradation of OII. The compounds obtained after calcination above 600 °C display the highest photocatalytic activity attributed to the formation of well crystallized ZnO and $ZnCr_2O_4$ spinel leading to complete mineralization of OII. Optimal photocatalytic conditions were defined as 0.5 g L^{-1} of photocatalyst and basic pH conditions. To further highlight the oxidation process, experiments with 4-chlorophenol, which is not adsorbed on LDH surface and with isopropanol and terephthalic acid, used as $HO^{\bullet}$ radical trap, were carried out. In terms of photodegradation mechanism, both hydroxyl radical generation in bulk and direct interaction with hole on the surface of the photocatalysts were evidenced.

1. Introduction

Recently, advanced oxidation processes (AOPs) have attracted a considerable attention as efficient methods allowing a complete mineralization of organic pollutants, compared to adsorption phenomena which are solely based on pollutant immobilization. Particularly, semiconductor based photocatalysts are of great interest for hazardous wastewaters remediation and toxic air contaminant reduction. In such processes, catalytic reactions are stimulated by UV and visible-light absorption which create in the materials electron–hole pairs, able to migrate to the surface and to further generate free radicals. Various materials such as TiO_2, WO_3, $SrTiO_3$, α-Fe_2O_3, ZnO, ZnS... have been described as effective photocatalysts [1]. Interestingly, layered double hydroxides (LDH) based photocatalysts combining adsorption feature and photocatalytic activity were also reported in the literature for organic pollutants degradation [2–5] and for visible light induced O_2 and H_2 generation from water [6–8]. LDH also named anionic clays belong to the family of layered compounds with the general formula $[M^{II}_{1-x}M^{III}_{x}(OH)_2]^{+x}[A_{m}{}^{-x/m}.nH_2O]$. They can be described by the association of divalent and trivalent cations in a brucite like layers with the presence of anions in the interlayer domain to compensate the positive charges of the layer. According to the formula, it is possible to obtain a great variety of LDH by solely changing the nature and proportions of the metallic cations in the hydroxyl sheets and by the intercalation of various solvated anions in between the layers [9]. Such chemical composition versatility joined with their anionic exchange properties opens for this class of compounds a wide range of application fields that include adsorption [10], catalysis [11], electrochemistry [12], medicine [13] and nanocomposites

* Corresponding author at: Clermont Université, Université Blaise Pascal, Institut de Chimie de Clermont-Ferrand, BP 10448, F-63000 Clermont-Ferrand, France. Tel.: +33 473407104; fax: +33 473407933.
E-mail address: vanessa.prevot@univ-bpclermont.fr (V. Prevot).

http://dx.doi.org/10.1016/j.apcatb.2015.01.029
0926-3373/

[14]. To design efficient LDH based photocatalyst, different strategies are reported in the literature. In one hand, LDH are merely considered as adsorbent materials suitable to immobilize semiconductor particles or homogenous photocatalysts [15–17] and to elaborate photocatalytic heterostructures. TiO_2, ZnO, SnO_2, Au particles were successfully immobilized at the LDH surface by different pathways such as simple mixing [18,19], impregnation [20–22], layer by layer deposition [23], delamination restacking [24], calcination-reconstruction [25–27]. For instance, Carja et al. reported that dyes photodegradation is greatly enhanced by the deposition of nanosized nickel particles on LDH platelets surface through LDH reconstruction process in $NiSO_4$ solution [5]. On the other hand, thanks to a judicious choice of LDH intralayer cations it is possible to tune their photochemical activity. Photo-efficient LDH compounds containing various transition elements such as Ti [28–30], Zn, Ga [31], In [32], Y [15], homogeneously dispersed into the LDH layers were investigated, showing high specific surface areas, high thermal stability and semiconducting properties. In particular, since ZnCr–LDH compound was reported as an efficient photocatalyst for visible light water splitting [8], a peculiar attention has been paid to Cr^{3+} based LDH [3,33–36]. In an elegant approach, Gunjakar et al. [7] used a self-assembly process to associate positively charged ZnCr nanosheets and negatively charged layered titanium oxide to improve the ZnCr – photocatalytic efficiency.

In this study, carbonate intercalated ZnCr–LDH has been prepared with the aim to better understand the mechanism of photocatalytic organic pollutant degradation. Orange II (OII) and 4-chlorophenol (4-CP) were used herein as models of adsorbing and non adsorbing organic molecules, respectively. Evolution of the physico-chemical features and photocatalytic properties of ZnCr–CO_3 phase calcined at different temperatures were deeply studied. The mineralization process for OII degradation was also analyzed conjointly with different parameters that can affect the photocatalytic processes such as pH of the solution and photocatalyst loading. Finally to get better insight on the photodegradation mechanism $HO^{\bullet}$ radicals generation was studied.

2. Experimental

2.1. Characterization

Powder X-ray diffraction patterns were recorded on a X'Pert Pro Philips diffractometer with diffracted beam graphite monochromator using Cu Kα radiation source in the 2θ range of 5–70° with a step of 0.013° and a counting time per step of 20 s. A high-temperature chamber (Anton Paar HTK 16) was used to record *in situ* high temperature measurements under ambient atmosphere. The measurements were carried out after 15 min equilibrium at each temperature and a heating rate of 5 °C/min was used. Attenuated total reflectance Fourier transform infrared (FT-IR) spectra were measured in the range of 400–4000 cm^{-1} on a FTIR Nicolet 5700 spectrometer (Thermo Electon Corporation) equipped with a Smart Orbit accessory. SEM characteristics of the samples were imaged by a JSM-7500F FESEM operating at 2 kV. Specimens were mounted on conductive carbon adhesive tabs. Transmission electron microscopy (TEM) images were taken using a JEOL JEM-2100F TEM microscope operated at 200 kV and coupled with an energy X-ray spectrometer (EDS). The zeta potential was measured using a Malvern Zetasizer Nano ZS (Mavern Instrument). Nitrogen adsorption–desorption experiments for surface and porosity quantification were performed at −196 °C with a Micromeritics ASAP 2020. Before analysis, samples were pretreated at 80 °C under vacuum for 12 h. The surface areas were estimated by using the Brunauer–Emmett–Teller method. Thermogravimetric analyses (TGA) were recorded on a Setaram TG-DTA 92 instrument in the temperature range of 25–1000 °C in air atmosphere, with a heating rate of 5 °C/min. Energy band gap of the synthesized materials was determined spectroscopically. Diffuse reflectance spectra of the power photocatalysts placed in 5 mm quartz cell were measured using UV/VIS/NIR spectrophotometer Lambda 19 (PerkinElmer) equipped with integrating sphere. The original coordinates of the spectra (reflectance *vs.* wavelength) were transformed to Kubelka–Munk function (K) *vs.* photon energy ($h\nu$) [37]. The final plots of $(K.h\nu)^{1/2}$ as a function of $h\nu$ are in accordance with the theoretical equation [38,39], $h\nu.\alpha$ = constant $(h\nu - E_{bg})^2$ where α is absorption coefficient of photocatalyst and E_{bg} its energy band gap. The values of energy band gap are estimated by extrapolation of the linear part of the dependence for ZnCr–CO_3. For derivative oxides, we employed a more precise method based on fitting of the experimental dependences by Boltzmann symmetrical function using non-linear regression. Then the calculated crossing point of the tangent line in the inflection point of the Boltzmann fit with its lower asymptote determines the energy band gap. For powders composed of two different crystallographic phases as LDH derived mixed oxides, the single Boltzmann function did not fit the experimental data well. In such cases, a double Boltzmann fit by a sum of two Boltzmann functions was applied. Mineralization of OII was monitored by measuring the total organic carbon concentration in using a TOC-5050A analyzer (Shimadzu). The amount of OII in solution was measured by UV–vis spectroscopy (Varian Cary 100 Scanning UV–vis spectrophotometer) by monitoring the absorbance at λ max = 483 nm. The amount of 4-CP was followed by high performance liquid chromatography using a Waters 2695 HPLC chromatograph equipped with a Waters 2998 photodiode array detector. A mobile phase methanol/water (50:50; v/v) was applied with a flow rate of 1 ml/min. Licrosphere RP-18 (5 μm) column (length 12.5 cm), with a guard column LichroCART 4-4, RP-18 (5 μm) (both Merck, Germany) was used.

2.2. Materials preparation

All the reagents were analytical grade and used without further purification. $Zn_2Cr(OH)_6Cl\,nH_2O$ LDH phase noted ZnCr–Cl was prepared by the coprecipitation method as reported elsewhere [40]. Briefly, a 1 mol L^{-1} mixed solution of metal chloride salts (Zn/Cr ratio of 2) was added drop wise into a reactor filled with deionised water under stirring. The pH value of the reactor solution was maintained constant at 5.5 by controlled NaOH (2 mol L^{-1}) addition. After complete addition of the salt solution, the precipitate was aged for 24 h at room temperature, isolated by centrifugation, washed three times with deionised water and dried under ambient atmosphere.

Then, $[Zn_2Cr(OH)_6]^+(CO_3^{2-})_{0,5}\,nH_2O$ hereafter noted ZnCr–CO_3 was obtained by anionic exchange from $[Zn_2Cr(OH)_6]^+\,Cl^-\,nH_2O$ phase. Typically, 5 g of chloride intercalated LDH solid was suspended in 500 mL of 0.1 M Na_2CO_3 solution and stirred for 12 h. After this time, the solid was recovered by centrifugation, washed three times with deionised water and air dried.

ZnCr–CO_3 was then calcined at different temperatures (300, 400, 500, 600, and 800 °C). The calcinations were done in an electric oven using a temperature ramp of 10 °C/min. Once the target temperature was reached, the sample was calcined for 4 h and left to cool down slowly in furnace.

2.3. Sorption experiments

Adsorption measurements were carried out using a batch method at a controlled temperature of 20 °C and the pH was initially fixed at 7.0 ± 0.5. The adsorption isotherms were recorded for 10 mL of 1 mg mL^{-1} solid suspensions in equilibrium with OII

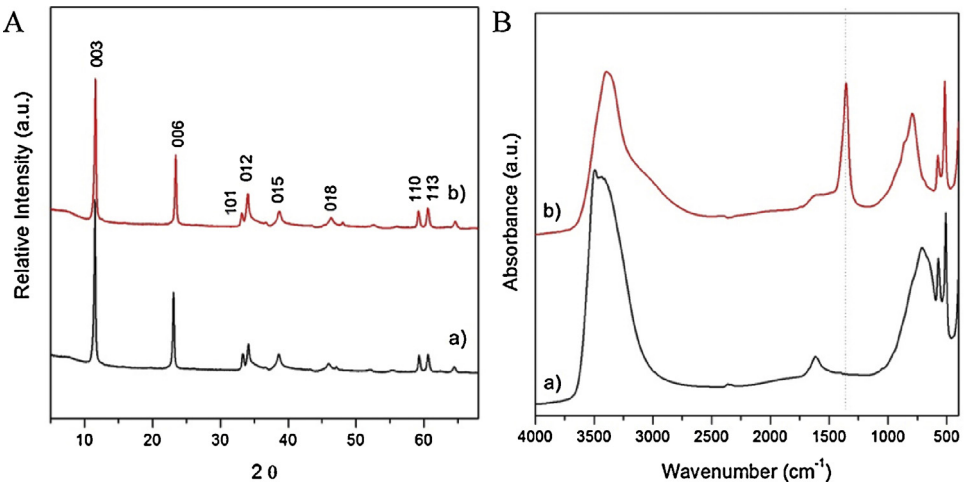

Fig. 1. (A) PXRD patterns and (B) FTIR spectra of (a) ZnCr–Cl and (b) ZnCr–CO_3.

concentrations ranging from 0 to 5 mmol L^{-1}. The suspensions were stirred at a constant speed (500 rpm) for 12 h and centrifuged at 4500 rpm for 30 min. OII concentration was estimated spectrophotometrically. The amount of OII adsorbed by the compounds, qe, was determined from the difference between the initial (Ci) and equilibrium (Ce) concentrations of the OII per gram of ZnCr based materials: qe = (Ci – Ce) V/m. The adsorption isotherms were obtained by plotting qe *vs.* Ce.

2.4. Measurement of photocatalytic activity

The photocatalytic efficiency was measured by degradation of OII and 4-CP as model pollutants. Experiments were performed with a constant sample concentration of 0.5 g L^{-1} if it is not mentioned differently, while the concentration of pollutants involved in the reaction, was systematically fixed at 5.10^{-5} mol L^{-1}. Typically, 0.03 g of ZnCr–CO_3 or derived mixed oxides was added to 60 mL of pollutants solution in dark for 1 h to attain the adsorption/desorption equilibrium on the photocatalyst surface. Then the irradiation was carried out under stirring conditions at room temperature. The irradiation setup used for both kinetics and analytical experiments consisted of an elliptical stainless steel cylinder. A high-pressure mercury lamp (Philips HPW type 125 W) was located at a focal axis of the elliptical cylinder. An inner filter permits to select a main emission at 365 nm (93%). A water-jacketed Pyrex tube (diameter = 1.8 cm) was used as reactor and centered at the other focal axis. At different time intervals, small volumes of suspension were taken out. Before to perform the absorbance measurement by UV–vis or HPLC, the pH was decrease to 2 by addition of few drops of concentrated acidic solution (HCl) in order to ensure the LDH dissolution and the release of adsorbed molecules in the solution. Then, disappearance measured only concerned the photodegradation. Blank experiment was carried out in parallel in the same conditions but in the absence of catalyst. According to the analysis, errors between 3 and 5% have to be taken into account.

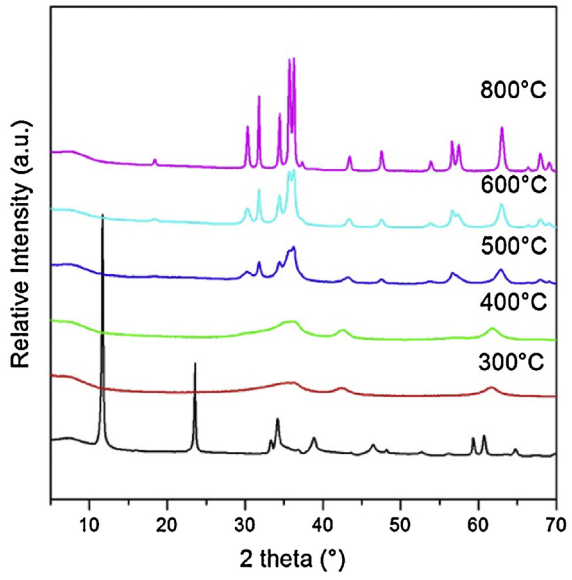

Fig. 2. PXRD patterns of ZnCr–CO_3 and the derived materials after calcination at different temperatures for 4 h.

To measure the photoproduction of HO• by LDH photocatalyst, the measurement reactivity of terephthalic acid (TA) was used [41]. 3 mL of photocatalyst (c = 0.5 g L^{-1}) and TA solution ($c = 5.10^{-5}$ mol L^{-1}) were irradiated in a stirred quartz cuvette under monochromatic light of different wavelengths (296, 313, 340, 365, 380, 400, and 450 nm) by monochromator equipped with a Xe 1000 W lamp (ORIEL) at room temperature. At fixed times during irradiation, the cuvette was removed and the suspension was centrifuged to remove the photocatalyst from the system and then transferred into measurement cuvette and the concentration of 2-hydroxyterephthalic acid (TAOH) was determined using PerkinElmer MPF 3 L spectrofluorimeter. The formation of HO• was monitored from the fluorescence of TAOH (λ_{exc} = 320 nm, λ_{em} = 420 nm), quantifiable using standard solutions.

3. Results and discussion

3.1. ZnCr based materials preparation and characterization

Carbonate intercalated LDH phases were considered as precursors of choice to produce derived mixed oxides due to the carbonate anions full decomposition at rather low temperatures. ZnCr–CO_3 was successfully prepared by coprecipitation of ZnCr–Cl followed by anionic exchange with carbonate anions. This two step method was preferred to the direct carbonate LDH phase preparation to ensure a high crystallinity level and purity of Cr based LDH phase, favored in rather acidic conditions of synthesis for such a composition [42]. Indeed, a high level of LDH crystallinity was reported to enhance the LDH photocatalytic activity [32]. Fig. 1A shows the XRD patterns of ZnCr–Cl and ZnCr–CO_3 samples both displaying the typical LDH structure reflections which can be indexed with a

hexagonal lattice and R-3m symmetry. The interlamellar distances deduced from the 00l diffraction lines correspond to 0.77 nm and 0.76 nm, respectively, for ZnCr–Cl and ZnCr–CO_3 which is in good agreement with the values reported in the literature [42]. Note that a Zn/Cr molar ratio of 2.3 for ZnCr–CO_3 was determined by EDS. This value is in quite good agreement with a complete coprecipitation of both zinc and chromium in the LDH phase as this ratio is near to the M^{II}/M^{III} ratio (2.0) of the starting metal salt solution involved in the coprecipitation process. Concerning the interlayer anion, the replacement of chloride by carbonate anions was more clearly evidenced on the FTIR spectra (Fig. 1B) by the presence after the anionic exchange reaction of an intense band at 1361 cm^{-1} characteristic of carbonate anion (ν_{CO3}), all the others bands characteristic of LDH layers such as ν_{OH} (3400 cm^{-1}), δ_{H2O} (1618 cm^{-1}), ν_{MO} (720, 570, and 508 cm^{-1}), being maintained.

To get further insight on the thermal behavior of LDH precursor compound, both TGA/DTG and high temperature *in situ* PXRD were studied. The TGA curve clearly reveals four main mass loss steps (see Supporting materials Fig. S1). The first one between 25 °C and 150 °C (3%) is correlated to the loss of surface adsorbed and interlayer water molecules. It allows to calculate a number of 0,5 H_2O mole per mole of LDH. The next two endothermic mass losses are partially overlapped with the main loss weight (24.2%/28.5%) corresponding to dehydroxylation of the hydroxide layers and partial anion decomposition. Indeed the final weight loss above 375 °C (3.1%) is less than what could be expected for theoretical complete anion decomposition (9%). From these results we inferred that the chemical formulae of the prepared products are, respectively, $Zn_{2.3}Cr(OH)_{6.6}Cl\ 0.7H_2O$ and $Zn_{2.3}Cr(OH)_{6.6}(CO_3)_{0.5}\ 0.5H_2O$. The PXRD patterns recorded *in situ* at different temperatures (Fig. S2) in quite similar heating rate conditions than for TGA, evidence that in the range of temperature between 30 °C and 150 °C, no significant change in the patterns are noticed evidencing that the removal of water molecules from the ZnCr LDH matrix and the moderate thermal treatment do not strongly modify the interlayer domain structure. Above 150 °C, the *in situ* PXRD patterns display very broad and ill-defined peaks evidencing that such temperature corresponding to the beginning of the dehydroxylation, induces the collapse of the dehydrated ZnCr–CO_3 which is converted to an amorphous phase. Characteristic diffraction lines of pure and mixed oxides (ZnO and $ZnCr_2O_4$) appear in the patterns for calcination of the sample above 600 °C. These latter become more intense and thinner upon a further increase of the temperature causing higher crystallization of $ZnCr_2O_4$ and ZnO.

In parallel, PXRD patterns were also recorded classically on samples calcined at various temperatures for 4 h (Fig. 2). It is noteworthy that in these thermal treatment conditions, oxides and mixed oxides crystallize at lower temperatures. At 500 °C, rather thin and well-defined diffraction lines of $ZnCr_2O_4$ and ZnO are already observed due to the prolonged thermal treatment at fixed temperatures which were not yet present in using *in situ* PXRD measurements. As expected, EDS measurements indicate that the Zn/Cr molar ratio (Table 1) is nearly the same, regardless of the thermal treatment applied to the matrix.

Due to the dehydroxylation of the LDH layer at moderate temperature inducing a huge change of the surface properties, the zeta potential of the particles decreases from +25 mV for the pristine ZnCr material to 0 mV after 4 h at 300 °C (Table 1), staying at similar values for treatment at higher temperatures. Concerning the evolution of the Brunauer–Emmett–Teller (BET) specific surface areas upon calcination, the values (Table 1) are significantly reduced above 500 °C. This trend is directly correlated to the oxides and mixed oxides crystallization.

Generally for LDH matrices, an maximum value of surface area is reached upon moderate thermal treatment (250–350 °C) corresponding to the formation of amorphous mixed oxides [43]. Such behavior is not observed for ZnCr composition probably due to the premature decomposition of hydroxyl layered previously

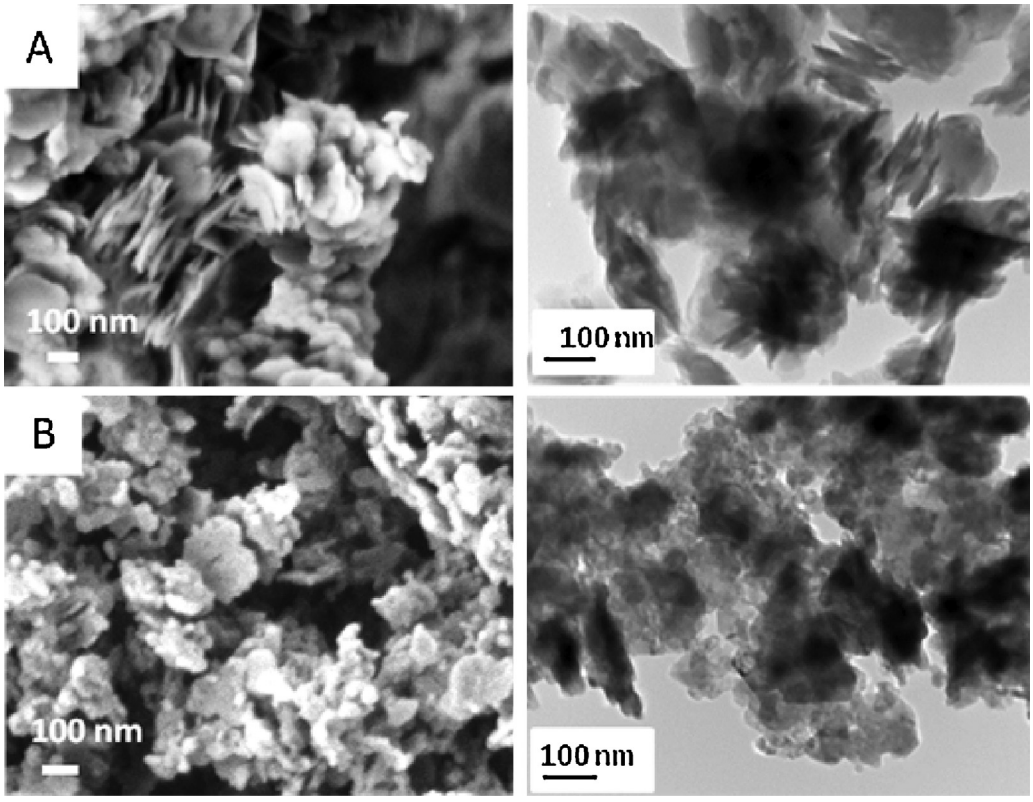

Fig. 3. FESEM (left) and TEM (right) images for (A) ZnCr–CO_3 and (B) ZnCr-600 °C.

Table 1
Zn/Cr molar ratio, surface area, porous volume, zeta potential and band gap for the ZnCr–CO_3 matrix and the calcined derivatives.

Sample	Zn/Cr ratio[a]	Zeta potential (mV) ± 5	S BET ($m^2 g^{-1}$) ± 2	Porous volume (cm^3)	Band gap (eV)
$ZnCrCO_3$	2.3	25	39	0.137	2.15
ZnCr-300 °C	2.4	0	40	0.140	0.69(54%)/2.5 (46%)
ZnCr-400 °C	2.3	3	36	0.147	1.3(58%)/2.6 (42%)
ZnCr-500 °C	2.3	3	29	0.108	1.7(37%)/2.9(63%)
ZnCr-600 °C	2.3	5	16	0.054	2.8(53%)/3.3(47%)
ZnCr-800 °C	2.3	5	7	0.013	2.4(40%)/3.3(60%)

[a] Determined by EDS.

evidenced by PXRD. ZnCr–CO_3 and ZnCr-600 °C exhibit type IV adsorption isotherms according to Rouquerol et al. [44] which are characteristic of mesoporous materials (Fig. S3).

The hysteresis loop is type H3 corresponding to slit shape pores usually observed for LDH materials due to the presence of aggregates of plate like particles. Such morphology is confirmed by SEM and TEM images presented in Fig. 3 which reveal for the uncalcined ZnCr–CO_3 precursor the presence of stacked plate-like particles with size in the range of 150–200 nm ± 20 nm. Because of the collapse of the layered structure and the oxides crystallization occurring at 600 °C, the particle size is clearly reduced on the SEM and TEM images, with the presence of smaller spherical oxide particles at the platelet surface.

3.2. Adsorption behavior

Prior to UV–vis irradiation, adsorption isotherms of OII on uncalcined and calcined ZnCr–CO_3 were recorded in dark. Indeed, LDH are well known for their high adsorption properties of anionic species [45–47]. The adsorption experiments were carried out for all the samples using the same procedure. Adsorption isotherms of OII molecules by ZnCr–CO_3 phase and calcined derivatives at 20 °C are presented in Fig. 4.

According to the classification proposed by Giles et al. [48] these isotherms correspond to the L-type adsorption reaction which are observed when the adsorbent surface is covered by independent adsorption sites which possess a high affinity for adsorbed molecules. Such behavior was previously described for OII adsorbed on MgAl LDH [49]. As under the pH conditions of adsorption (7.0), the OII is in the anionic form then the adsorption process corresponds to an anion exchange equilibrium.

The pristine LDH displays the greater adsorption properties, saturation of the surface is obtained at equilibrium value Ce of 2.5 mol L^{-1}. At the plateau value, the adsorption does not exceed 59.32% of the total anion exchange capacity, 41% of the intercalated CO_3^{2-} anions remain still unaccessible. With the increasing temperature of calcination, the amount of adsorbed OII on the sample surface is decreasing. For the calcined samples, plateau are reached at very low equilibrium concentration (<0.5 mol L^{-1}) and lower adsorption capacities were obtained (Table 2). For all the samples no further adsorption is observed at higher concentrations (>4 mol L^{-1}). This trend indicates that the interactions between dye molecules and inorganic powder are stronger than the sorbent–sorbent interactions. Percentage of anion exchange capacity decreases progressively.

Table 2
Results on adsorption properties obtained from isotherms using a Langmuir model.

Materials	ZnCr–CO_3	ZnCr-500 °C	ZnCr-600 °C	ZnCr-800 °C
Qmax (mg/mg)	0.585	0.176	0.136	0.116
% a.e.c.[a]	59.32	17.85	13.79	6.88
r^2	0.992	0.995	0.999	0.999

[a] Anionic exchange capacity.

After the OII adsorption on ZnCr–CO_3 and ZnCr-600 °C, all the diffraction lines on PXRD patterns are unmodified (Fig. S4), evidencing that OII molecules are adsorbed at the particle surface but not intercalated into the layered structure. Such behavior is in good agreement with the high affinity of carbonate anions for LDH matrix and the great structural cohesion between ZnCr positive layers and $[(CO_3^{2-})_{0.5}\cdot nH_2O]$ negative interlayer. Similarly for ZnCr-600 °C phase, adsorption phenomenon does not modify the structure and since well crystallized oxides are already formed, no regeneration phenomenon is observed. However, on the PXRD patterns a peak at $\theta = 18°$ appears with increasing OII concentration traducing crys-

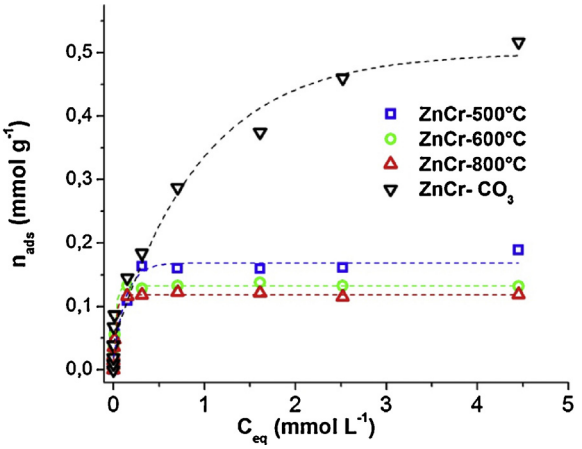

Fig. 4. OII adsorption isotherms for ZnCr–CO_3, ZnCr-500 °C, ZnCr-600 °C and ZnCr-800 °C.

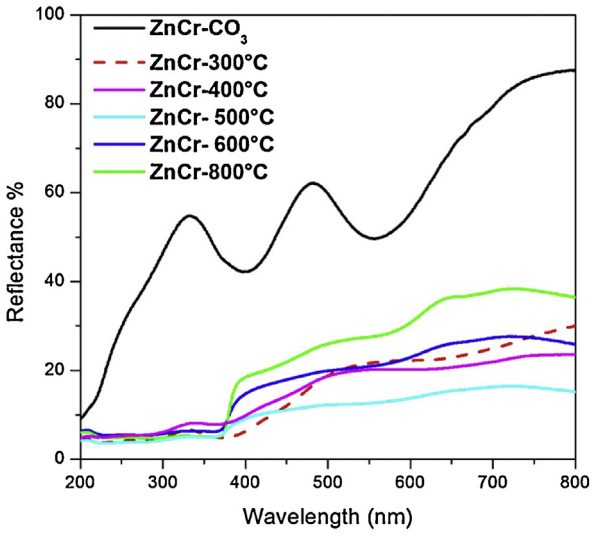

Fig. 5. UV–vis diffusive reflectance spectra of ZnCr–CO_3 and the derived materials after calcination at different temperatures for 4 h.

Table 3
Degradation rate of OII in first 60 min of irradiation for ZnCr–LDH calcined at different temperatures and with different loading (0.25, 0.5 or 1 g L^{-1}).

$t_{calcination}$ (°C)	None	300	400	500	600	800
r_i (mol min^{-1}), 0.25 g L^{-1}	–	–	–	–	3.74×10^{-9}	–
r_i (mol min^{-1}), 0.5 g L^{-1}	3.70×10^{-9}	6.22×10^{-10}	4.86×10^{-9}	8.47×10^{-9}	9.25×10^{-9}	9.77×10^{-9}
r_i (mol min^{-1}), 1.0 g L^{-1}	–	–	–	–	9.79×10^{-9}	–

tallization of a side inorganic hydroxide phase due to probably a partial LDH or oxides hydrolysis. In any cases, all the calcined phases keep some adsorption sites.

3.3. Light absorption properties

The band gap of calcined ZnCr–CO_3 samples were calculated from UV reflectance spectra (Fig 5). Since LDH derived oxides combine ZnO particles and $ZnCr_2O_4$ spinel phase, a double Boltzmann fit by a sum of two Boltzmann functions was applied to determine the band gap (see Fig. S5 ESM). The values obtained for calcined derivatives were reported in Table 1. The lowest values correspond to the spinel phase whereas the highest can be attributed to the ZnO particles which is well-known as a large band gap semi-conductor (3.2–3.4 eV).

The increase of the calcination temperature leads to the increase of the calculated band gap value. This trend indicates that calcinations which induce the oxide crystallization strongly influence the absorptive properties of the resulting materials. It should be underlined that for higher calcination temperature, the phase displaying the higher band gap value is favored.

3.4. Photocatalytic activity

3.4.1. Effect of calcination temperature and loading

The photocatalytic activities of ZnCr–CO_3 LDH, uncalcined and calcined at 300, 400, 500, 600 and 800 °C, were evaluated by the photodegradation of OII under UV light irradiation. Their photodegradative efficiencies were measured at fixed pH value of 7. The results are reported in Table 3 and Fig. 6. Interestingly pristine ZnCr–CO_3 LDH displays photocatalytical properties leading to 34% of OII degradation after 5 h. Obviously, the calcination temperature has significant influence on photocatalytic activity of ZnCr–LDH. A moderate thermal treatment lower than 500 °C induces a net decrease of the photocatalytic activity, whereas for calcined ZnCr–CO_3 at higher temperatures (500 °C, 600 °C and 800 °C) the photoactivity increases. Note that for calcinations at 600 °C and 800 °C, the rate of the degradation is the same. These results indicate that both hydroxylated LDH layers and well-crystallized ZnO based derivative mixed oxides can act as photocatalyst.

The photocatalyst concentration also takes an important role in the degradation of OII. As the calcined sample ZnCr-600 °C exhibited higher photoactivity, different doses of this photocatalyst were tested (0.25, 0.5 and 1 g L^{-1}) at pH 7 (Table 3). It was found that with amount of 0.5 g L^{-1} the degradation rate of OII is notably higher than with 0.25 g L^{-1}. A further increase of photocatalyst amount does not improve the OII degradation. After 5 h, 36%; 62% and 65% of OII degradation was obtained, respectively, for loading of 0.25, 0.5 and 1 g L^{-1} (Fig. S5). The amount of 0.5 g L^{-1} appears then as a good compromise between the photoefficiency and the screening effect of the materials in solution.

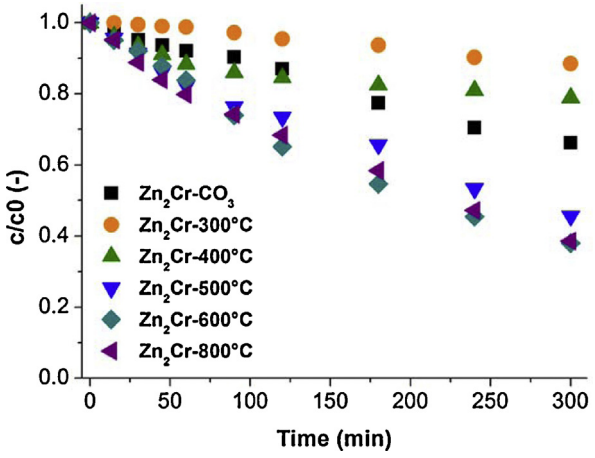

Fig. 6. Photodegradation of OII by ZnCr–CO_3 calcined at different temperatures (pH 7), [composite] = 0.5 g L^{-1}.

3.4.2. Effect of pH

The influence of pH on the photocatalytic degradation was also studied in the range of pH 5–9.5 for a dye concentration of 5.10^{-5} mol L^{-1} and a catalyst loading of 0.5 g L^{-1} (Table 4 and Fig. S6). For non calcined sample ZnCr–CO_3, higher is the pH value lower is the initial rate of OII degradation (Table 4). After five hours, for pH between 5 and 8 almost 34% of the dye is degraded compared to 20% at pH 9.5. To get a better insight on the pH effect, before each of photocatalytic tests, the reaction system was kept without UV irradiation for half an hour to reach the adsorption equilibrium. It was found that OII adsorption corresponds to 28% of total OII in solution at pH 5, 25%, at pH 6–8 and only 18% at pH 9.5. At lower pH the higher photocatalytic efficiency observed can then be explained by higher adsorption capacity due to the change of surface charge of photocatalyst. At pH 9.5, the pH is higher than pzc of ZnCr–CO_3

Table 4
Degradation rate of OII in first 60 min of irradiation at different pH, in presence of ZnCr–CO_3 and ZnCr-600 °C and corresponding degradation pourcentage after 5 h.

	pH	5	6	7	8	9.5
ZnCr–CO_3	Adsorption[a]	28%	25%	25%	25%	18%
	r_i (mol min^{-1})	8.00×10^{-9}	5.59×10^{-9}	3.70×10^{-9}	3.82×10^{-9}	2.86×10^{-9}
	Degradation[b]%	38%	32%	34%	32%	20%
ZnCr-600 °C	Adsorption[a]	5%	5%	6%	6%	7%
	r_i (mol min^{-1})	8.07×10^{-9}	7.51×10^{-9}	8.00×10^{-9}	7.50×10^{-9}	9.77×10^{-9}
	Degradation[b]%	33%	54%	62%	65%	60%

[a] Dark 1 h.
[b] After 5 h.

Table 5
Concentration of HO• radicals in first 15 min of measurement.

Sample	ZnCr–CO_3	ZnCr-600 °C					
Wavelength (nm)	365	296	313	340	365	380	400	450
$c_{15\,min}$(mol (L μW)$^{-1}$) 10^{-9}	0.07	6.29	5.76	4.35	1.60	0.41	0.07	0.05

(pzc = 8.5) [50], the anionic dye is then less attracted to the photocatalyst surface. The decrease of OII adsorption can also partially be attributed to a competitive adsorption of carbonate anions generated in such basic conditions. Indeed at lower pH, CO_3^{2-}/OII anion exchange is assisted by carbonate protonation.

It is noteworthy that in presence of calcined ZnCr-600 °C sample, whatever the pH similar initial rates are measured. However for longer irradiation time (5 h), the photodegradation is much less efficient at pH 5 with 33% of degradation compare to other pH (54–65%). The calcination of LDH and the formation of mixed oxides lead to a more photoactive materials at neutral or slightly basic pH.

3.5. Study of the reaction mechanism

In attempt to describe the possible contribution of oxidative species (HO• radicals) during the photocatalytic degradation, terephthalic acid was used to determine photoproduction of HO• radicals. In parallel, the isopropanol was used as a scavenger for HO• radicals to verify if the HO• radicals are the only oxidation species involved in the process. Note that to evaluate photocatalyst surface contribution, in addition to OII 4-CP was also used as a non adsorbing model compound.

At first, the photoproduction of HO• radicals was measured by reaction with terephthalic acid and the formation of hydroxyterephthalic acid [41]. The concentration of HO• radicals is measured in first 15 min and for a matter of comparison, the concentration was recalculated for the same light intensity per μW. The results (Table 5) proved that HO• radicals are photoproduced for both noncalcined and calcined samples at 365 nm. However, the HO• radical production is much more favored in the case of the calcined materials (around 23 times higher) in good agreement with the higher OII photodegradation previously observed (Fig. 6). These results show that HO• radical is the main oxidant species generated in the photocatalytic process with such materials.

For ZnCr-600 °C, the rate of HO• radical production is calculated at different wavelengths (Table 5). The lower the wavelength, the higher the HO• production is. For a wavelength lower than 340 nm, the production was around 2 orders of magnitude higher than for 450 nm. Clearly, the increase of energy favors the release of HO• radicals in solution, as previously observed with iron complexes [51].

As another step, tests were performed by inhibition of HO• radicals by reaction in the presence of isopropanol, known as an efficient way to check if the HO• radicals are the only oxidation species in the reaction [52]. For calculation, a negligible adsorption of isopropanol on material surface is considered. Fig. 7 displays the results obtained for the samples ZnCr–CO_3 and ZnCr-600 °C.

For ZnCr–CO_3 photocatalyst (Fig. 7a), it is obvious that the isopropanol has an influence on the degradation of OII. The use of 1 mol L^{-1} isopropanol leads to a net decrease of the OII degradation rate. The percentage of OII degraded after 5 h of irradiation passed from 34% to 11% in presence of isopropanol. From the Fig. 7b, in presence of ZnCr-600 °C, the use of increasing concentration of isopropanol in the range of 0–1 mol L^{-1} induces a progressive decrease of OII photodegradation, respectively, from 62% to 24% after 5 h. It is important to underline that even in presence of high concentration of isopropanol (1 mol L^{-1}) the OII degradation did not stopped completely for both samples.

For the better understanding of reaction mechanism, 4-CP was used as another model compound. After 0.5 h in dark in presence of LDH 4-CP concentration did not decrease confirming that 4-CP did not adsorbed on the surface of photocatalyst. Photodegradation experiments were then performed with both ZnCr–CO_3 and ZnCr-600 °C at pH 7. The results are shown in Fig. 8. ZnCr–CO_3 did not show any photoactivity toward 4-CP, evidencing that the amount of photoproduced HO• radicals was too low. After 5 h for calcined sample, a 4-CP degradation of 35% was observed which was around two times lower than the degraded amount of OII using the same starting conditions. When the degradation was carried out with sample ZnCr-600 °C in the presence of 1 mol L^{-1} isopropanol, the reaction was almost stopped and the amount of 4-CP decreased only for around 4%.

Then clearly, in presence of a model compound not adsorbed on the mixed oxides photocatalyst surface, only HO• radicals, *i.e.,* the bulk mechanism is involved. On the contrary, when the organic compound has a higher affinity with the LDH derivative photocatalyst (which means mainly higher adsorption), two oxidation mechanisms, namely hydroxyl radical mechanism in bulk and direct hole mechanism on the surface of the photocatalyst proceed simultaneously. However, we can estimate that the HO• radical mechanism in the bulk is the predominant mechanism for

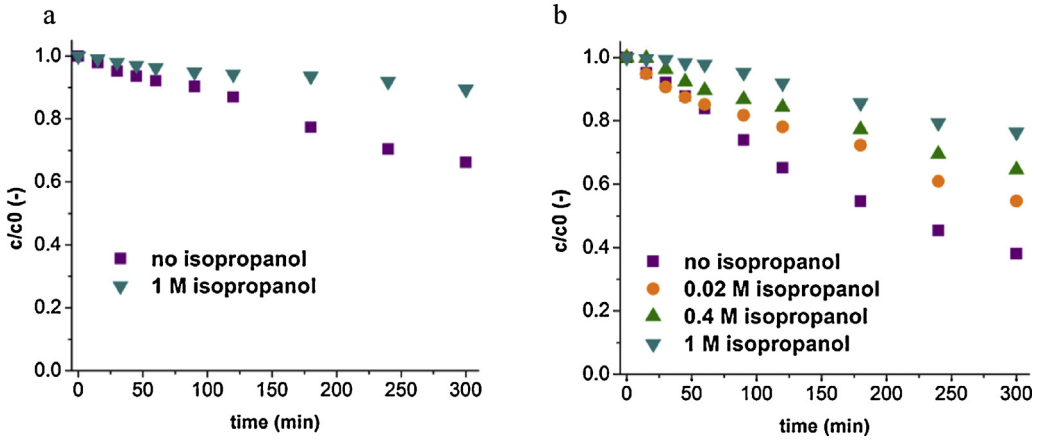

Fig. 7. Influence of isopropanol addition to reaction system, (a) ZnCr–CO_3 0.5 g L^{-1}, (b) ZnCr-600 °C 0.5 g L^{-1}.

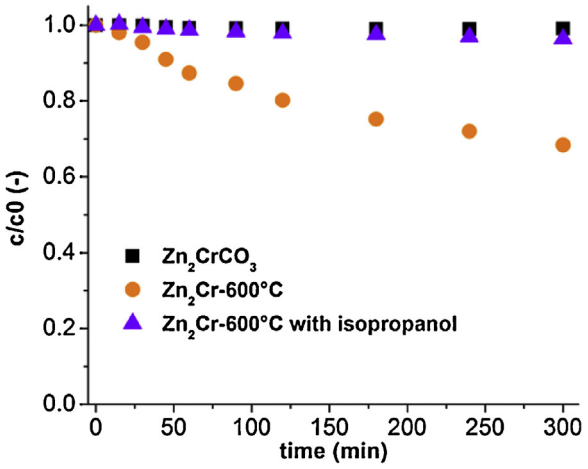

Fig. 8. Degradation of 4-CP by ZnCr–CO_3 and ZnCr-600 °C (reaction carried out without and with isopropanol 1 M).

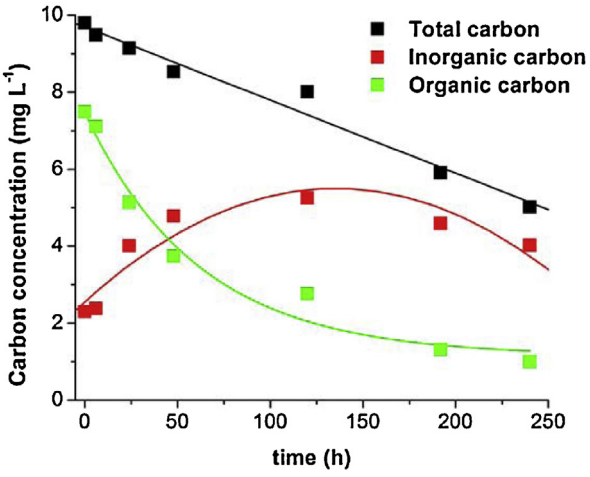

Fig. 9. TOC measurements of OII (5.10^{-5} mol L^{-1}) degradation by ZnCr-600 °C (0.5 g L^{-1}).

the oxidation of organic compound compared with direct hole contribution with 68% and 61% (around 2/3) of total OII degradation, respectively, for pristine $ZnCrCO_3$ and ZnCr-600 °C.

3.6. Study of complete mineralization

To see if the OII undergoes complete mineralization by degradation with ZnCr-600 °C total organic carbon (TOC) measurements were performed. The results are shown in Fig. 9. It is obvious that the organic carbon concentration decreases with irradiation time. In parallel, formation of inorganic carbon is evidenced until 120 h corresponding to transformation of organic carbon into inorganic species (hydrogenocarbonate and carbonate). For longer irradiation time the concentration of inorganic carbon starts also to decrease. Globally, the total carbon concentration decreases progressively with the time of irradiation from 9.8 to 5.0 mg L^{-1} after 240 h. Since remaining carbon is mainly inorganic carbon, this result evidences that the degradation by ZnCr-600 °C leads to total or quasi total mineralization of OII.

4. Conclusions

Photocatalytic activity of ZnCr–CO_3 LDH and derivative mixed oxides prepared by calcinations was studied. Both forms non calcined and calcined induce OII phtotdegradation with different efficiency. The influence of various parameters such as loading, pH and wavelength were evidenced. Thanks to the use of two model compounds (OII and 4-CP), terephthalic acid and isopropanol the photocatalytic mechanism was highlighted. Obviously both photocatalysts are able to produce HO• radicals under the UV light irradiation. However, HO• radicals are not the only oxidising species participating in the photocatalytic reaction. According to the measurements, it appears that the ongoing reaction in this system is based on two simultaneous reactions: the HO• radicals oxidation in one side and direct hole reaction on the photocatalyst surface on the other side. With this study, it is possible to estimate that HO• radical is responsible of around 2/3 of the OII oxidation process. Moreover, our results show that such photocatalysts are more efficient for the decomposition of organic molecules with good affinity to LDH surface.

Appendix A. Supplementary data

Supplementary data associated with this article can be found, in the online version, at http://dx.doi.org/10.1016/j.apcatb.2015.01.029.

Referencesee queries 5 and 6s

[1] A. Di Paola, E. Garcia-Lopez, G. Marci, L. Palmisano, J. Hazard. Mater. 211–212 (2012) 3–29.
[2] K.M. Parida, L. Mohapatra, Chem. Eng. J. (Amsterdam, Neth.) 179 (2012) 131–139.
[3] K. Parida, L. Mohapatra, N. Baliarsingh, J. Phys. Chem. C 116 (2012) 22417–22424.
[4] S. He, S. Zhang, J. Lu, Y. Zhao, J. Ma, M. Wei, D.G. Evans, X. Duan, Chem. Commun. (Cambridge, U. K.) 47 (2011) 10797–10799.
[5] G. Carja, E. Husanu, C. Gherasim, H. Iovu, Appl. Catal. B 107 (2011) 253–259.
[6] K. Parida, M. Satpathy, L. Mohapatra, J. Mater. Chem. 22 (2012) 7350–7357.
[7] J.L. Gunjakar, T.-W. Kim, H.-N. Kim, I.-Y. Kim, S.-J. Hwang, J. Am. Chem. Soc. 133 (2011) 14998–15007.
[8] C. Gomes-Silva, Y. Bouizi, V. Fornes, H. Garcia, J. Am. Chem. Soc. 131 (2009) 13833–13839.
[9] V. Rives, Clay Miner. 41 (2006) 879.
[10] F. Bruna, R. Celis, I. Pavlovic, C. Barriga, J. Cornejo, M.A. Ulibarri, J. Hazard. Mater. 168 (2009) 1476–1481.
[11] A. Guida, M.H. Lhouty, D. Tichit, F. Figueras, P. Geneste, Appl. Catal. A 164 (1997) 251–264.
[12] C. Mousty, F. Leroux, Recent Pat. Nanotechnol. 6 (2013) 174–192.
[13] J.-H. Choy, M. Park, J.-M. Oh, Curr. Nanosci. 2 (2006) 275–281.
[14] F. Leroux, J.-P. Besse, Chem. Mater. 13 (2001) 3507–3515.
[15] L. Mohapatra, K.M. Parida, M. Satpathy, J. Phys. Chem. C 116 (2012) 13063–13070.
[16] E. Geraud, S. Rafqah, M. Sarakha, C. Forano, V. Prevot, F. Leroux, Chem. Mater. 20 (2008) 1116–1125.
[17] L. Mohapatra, K.M. Parida, Phys. Chem. Chem. Phys. 16 (2014) 16985–16996.
[18] E.M. Seftel, E. Popovici, E. Beyers, M. Mertens, H.Y. Zhu, E.F. Vansant, P. Cool, J. Nanosci. Nanotechnol. 10 (2010) 8227–8233.
[19] S.P. Paredes, M.A. Valenzuela, G. Fetter, S.O. Flores, J. Phys. Chem. Solids 72 (2011) 914–919.
[20] E. Dvininov, M. Ignat, P. Barvinschi, M.A. Smithers, E. Popovici, J. Hazard. Mater. 177 (2010) 150–158.
[21] Y. Zhi, Y. Li, Q. Zhang, H. Wang, Langmuir 26 (2010) 15546–15553.
[22] S. Yuan, Y. Li, Q. Zhang, H. Wang, Colloids Surf. A 348 (2009) 76–81.
[23] J. Han, Y. Dou, M. Wei, D.G. Evans, X. Duan, RSC Adv. 2 (2012) 10488–10491.
[24] Š. Paušová, J. Krýsa, J. Jirkovský, G. Mailhot, V. Prevot, Environ. Sci. Pollut. Res. 19 (2012) 3709–3718.
[25] R. Lu, X. Xu, J. Chang, Y. Zhu, S. Xu, F. Zhang, Appl. Catal. B 111–112 (2012) 389–396.
[26] G. Carja, A. Nakajima, S. Dranca, C. Dranca, K. Okada, J. Phys. Chem. C 114 (2010) 14722–14728.
[27] G. Carja, M. Birsanu, K. Okada, H. Garcia, J. Mater. Chem. A 1 (2013) 9092–9098.
[28] Y. Zhao, P. Chen, B. Zhang, D.S. Su, S. Zhang, L. Tian, J. Lu, Z. Li, X. Cao, B. Wang, M. Wei, D.G. Evans, X. Duan, Chem. Eur. J. 18 (2012) 11949–11958.
[29] M. Shao, J. Han, M. Wei, D.G. Evans, X. Duan, Chem. Eng. J. (Amsterdam, Neth.) 168 (2011) 519–524.
[30] Y. Lee, J.H. Choi, H.J. Jeon, K.M. Choi, J.W. Lee, J.K. Kang, Energy Environ. Sci. 4 (2011) 914–920.
[31] N. Ahmed, M. Morikawa, Y. Izumi, Catal. Today 185 (2011) 263–269.
[32] K. Teramura, S. Iguchi, Y. Mizuno, T. Shishido, T. Tanaka, Angew. Chem. Int. Ed. 51 (2012) 8008–8011, S8008/8001–S8008/8009.

[33] Y. Zhao, S. Zhang, B. Li, H. Yan, S. He, L. Tian, W.J. Shi Ma, M. Wei, D.G. Evans, X. Duan, Chem. Eur. J. 17 (2011) 13175–13181, S13175/13171–S13175/13112.
[34] L. Mohapatra, K.M. Parida, Sep. Purif. Technol. 91 (2012) 73–80.
[35] N. Baliarsingh, L. Mohapatra, K. Parida, J. Mater. Chem. A 1 (2013) 4236–4243.
[36] N. Baliarsingh, K.M. Parida, G.C. Pradhan, Ind. Eng. Chem. Res. 53 (2014) 3834–3841.
[37] R.B. Draper, M.A. Fox, Langmuir 6 (1990) 1396–1402.
[38] M. Grätzel, Photocatalysis, in: N. Serpone, E. Pelizzetti (Eds.), Fundamentals and Applications, Wiley, New York, 1989, p. 123.
[39] N.S. Lewis, M.L. Rosenbluth, in: N. Serpone, E. Pelizzetti (Eds.), Photocatalysis: Fundamentals and Applications, Wiley, New York, 1989, p. 99.
[40] H. Roussel, V. Briois, E. Elkaim, R.A. de, J.-P. Besse, J.-P. Jolivet, Chem. Mater. 13 (2001) 329–337.
[41] T. Charbouillot, M. Brigante, G. Mailhot, P.R. Maddigapu, C. Minero, D. Vione, J. Photochem. Photobiol. A 222 (2011) 70–76.
[42] C. Forano, U. Costantino, V. Prévot, C. Taviot Gueho, Handbook of Clay Science Developments in Clay Science, in: F. Bergaya, G. Lagaly (Eds.), Elsevier, 2013, pp. 745–782.
[43] V. Prevot, C. Forano, J.P. Besse, Chem. Mater. 17 (2005) 6695–6701.
[44] F. Rouquerol, J. Rouquerol, K.S.W. Sing, Adsorption by powders and porous solids, in: Principles Methodology and Applications, Academic Press, London, 1999.
[45] A.N. Ay, B. Zümreoglu-Kuran, A. Temel, Micropor. Mesopor. Mater. 98 (2006) 1.
[46] G.P. Gillman, Sci. Total Environ. 366 (2006) 926–931.
[47] K. Xing, H. Wang, L. Guo, W. Song, Z. Zhao, Colloids Surf. A 328 (2008) 15–20.
[48] C.H. Giles, D. Smith, A. Huitson, J. Colloid Interface Sci. 47 (1974) 755–765.
[49] M. Mustapha Bouhent, Z. Derriche, R. Denoyel, V. Prevot, C. Forano, J. Solid State Chem. 184 (2011) 1016–1024.
[50] L. Mohapatra, K.M. Parida, Sep. Purif. Technol. 91 (2012) 73–80.
[51] J. Li, G. Mailhot, F. Wu, N. Deng, J. Photochem. Photobiol. A 212 (2010) 1–7.
[52] C. Richard, F. Bosquet, J.F. Pilichowski, J. Photochem. Photobiol. A 108 (1997) 45–49.